MODELLING HIGH TEMPERATURE MECHANICAL PROPERTIES AND MICROSTRUCTURE EVOLUTION IN NI-BASED SUPERALLOYS

N. Saunders, Z. Guo, A. P. Miodownik and J-Ph. Schillé

Sente Software Ltd., Surrey Technology Centre, The Surrey Research Park, Guildford GU2 7YG, U.K.

Keywords: Modelling, JMatPro, γ' Microstructure, Mechanical Properties, High Temperature Flow Stress, Fatigue

Abstract

The present paper provides details on the development of models for calculating the material properties of Ni-based superalloys and makes extensive comparison of calculated results against experiment. The first part of the paper concentrates on extending a previously reported capability for the calculation of mechanical properties, such that strain rate dependent flow stress curves can be calculated from room temperature to the liquid state. Subsequent application to modelling of fatigue properties is briefly discussed. The second part concentrates on extending kinetic formalisms to calculate the volume, size and distribution of γ' in wrought and cast alloys, which are subsequently used in the prediction of mechanical properties as a function of heat treatment.

Introduction

Work on the development of modelling tools to calculate the material properties of multi-component Ni-based superalloys has been presented at previous Superalloy meetings [1,2,3]. The use of such modelling has become quite widespread through the development of the software programme JMatPro, providing significant benefit to many users and producers of Ni-based superalloys.

The present paper reports on recent technical work that has extended the capability of JMatPro [3] to (i) model high temperature, strain rate dependent flow stress curves, with subsequent application to the calculation of fatigue properties and (ii) the development of microstructure models for calculating the volume, size and distribution of γ' in wrought and cast alloys that can subsequently be used in the prediction of mechanical properties. In each case calculated results will be compared with experiment.

High Temperature Mechanical Properties

Previous work on modelling the mechanical properties of Ni-based superalloys [3,4] has concentrated on predicting proof and tensile strength as a function of temperature and strain rate, as well as creep properties [5]. Generally speaking, room temperature (RT) strength decays monotonically with increasing temperature until the point where it enters into a temperature regime where there is a sharp fall in strength and where flow stress then becomes much more strongly dependent on strain rate. This sharp drop in strength is due to a change from a deformation mechanism dominated by dislocation glide (DDG) at low temperatures to one dominated by dislocation climb (DDC) at higher temperatures, where the latter is usually the controlling mechanism for creep.

JMatPro employs different strength models to account for these two different mechanisms and whichever has the lower resistance to deformation controls the final strength of the alloy [3,4]. The two regions are clearly shown in Fig.1, using Nimonic 75 and 105 as examples. As can be seen good agreement with experimental data [6] is observed and the work was extensively validated against reported results [7] for a wide range of commercial alloys (see for example Fig.2).

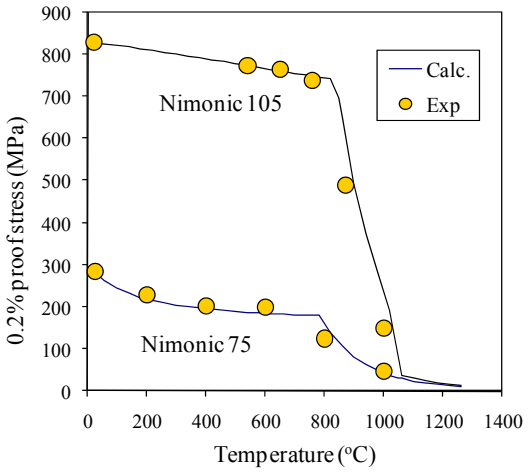

Figure 1. Comparison between experimental [6] and calculated 0.2% proof stress for Nimonic 75 and 105 as a function of temperature.

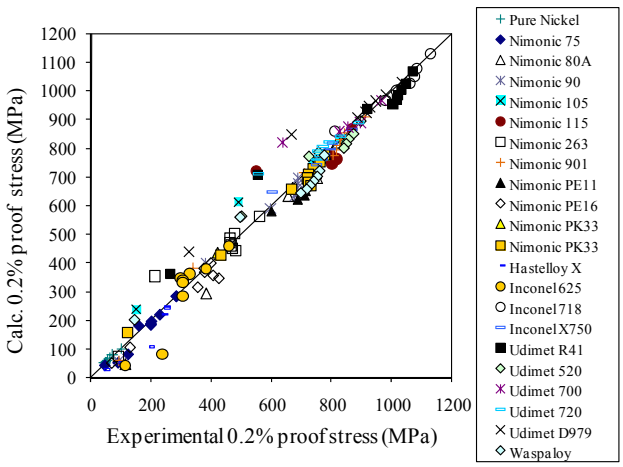

Figure 2. Comparison between experimental [7] and calculated 0.2% proof stress for various wrought superalloys and pure Ni between RT and 1000°C.

While such predictions have great value in their own right, they are limited when applied to deformation processes occurring during thermo-mechanical processing and fatigue, both of which require flow stress vs. strain diagrams. To this end the creep modelling has been extended such that flow stress vs. strain diagrams can be calculated for Ni-based superalloys both as a function of temperature and strain rate.

Flow stress diagrams

A capacity for calculating stress/strain curves is already available in JMatPro for the low temperature DDG regime utilising standard formulae [8]. However, no such formulae exist for creep. To remedy this shortcoming the secondary creep model has been extended to include primary and tertiary creep. It is, therefore, now possible to calculate full creep curves as a function of applied stress, which then allows the construction of a 3-dimensional surface that has as its axes stress, strain and time.

Assuming that the strain-rate in a tensile test and the creep rate in creep testing are interchangeable, it is then possible to calculate stress/strain curves at specific strain rates. Combining this procedure with stress/strain curves calculated for the DDG region allows stress/strain curves to be calculated over the full range of temperatures, including in the mushy zone.

The model for primary creep follows the work of [9] which uses the following relationship:

$$\dot{\varepsilon}_p = \frac{\dot{\varepsilon}_s}{K} \ln\left[1 + \frac{\dot{\varepsilon}_i - \dot{\varepsilon}_s}{\dot{\varepsilon}_s}(1 - e^{-Kt})\right] \quad (1)$$

where $\dot{\varepsilon}_p$ and $\dot{\varepsilon}_s$ are respectively the primary and secondary creep rates, $\dot{\varepsilon}_i$ is the initial creep rate and K is an empirically evaluated materials constant. In the present case we have made $\dot{\varepsilon}_i = \beta\dot{\varepsilon}_s$, [10] where β is a simple proportionality constant.

To account for tertiary creep we have used a somewhat empirical model that relates the tertiary creep rate to the secondary rate and the creep rupture life.

$$\dot{\varepsilon}_t = \dot{\varepsilon}_s\left[2C_d\, t(t / R_l)^4\right] \quad (2)$$

where $\dot{\varepsilon}_t$ is the tertiary creep rate, C_d is a "damage constant" and R_l is the rupture life, which can be readily calculated from the secondary creep rate and a Monkman-Grant type relationship [3,5].

The solution of Eqs.1&2 relies on prior knowledge of the secondary creep rate ($\dot{\varepsilon}_s$), which has been calculated using work reported earlier [3,5],

$$\dot{\varepsilon}_s = AD_{eff}\left(\frac{\gamma_{SFE}}{Gb}\right)^m\left(\frac{\sigma - \sigma_o}{E}\right)^n \quad (3)$$

where A is a materials dependent parameter, D_{eff} is the effective diffusion coefficient, γ_{SFE} is the stacking fault energy of the matrix at the temperature of creep, b is the Burgers vector, σ is the applied stress, σ_0 is the "back stress", with G and E, respectively, the shear and Young's modulus of γ at the creep temperature. The back stress σ_o, is calculated following the treatment of Lagneborg and Bergman [11], setting $\sigma_o = 0.75\sigma$ when $\sigma < 4\sigma_p/3$, (where σ_p is the critical back stress from strengthening due to precipitates) and $\sigma_o = \sigma_p$ when $\sigma > 4\sigma_p/3$. The exponents m and n are given a range of values in the literature, and in the present approach have been given fixed values of m=3 and n=4.

The calculated behaviour of alloys in the high temperature γ phase field can be used to demonstrate our approach. This is the region where such alloys are thermo-mechanically processed and where the modelling is likely to have most application. Fig. 3 shows creep curves for alloy 718 at various applied stresses at 1000ºC. In this case, the creep curve is calculated for true stress conditions, but it is possible to also calculate for constant load.

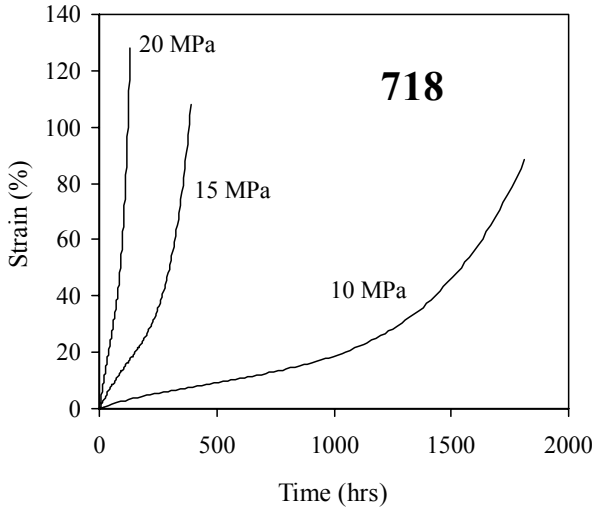

Figure 3. Calculated creep curves for a 718 alloy at 1000ºC.

The curves exhibit a classical shape, with a clearly resolvable primary creep region that decays to leave a period of "steady state creep", but which in reality already has some contribution from tertiary creep. The final rapid increase in strain rate leads to failure.

By tracking the 3-dimensional surface of stress/strain/time at a given temperature and a constant strain rate, it is possible to calculate the flow stress as a function of time and strain, which directly provides a flow stress diagram. The model has been developed and tested for a wide range of alloy types, including steels and Ti-alloys as well as Ni-based superalloys [12,13].

A noticeable feature of the present work is that flow softening at high temperatures arises as a direct result of the calculations. As such three regions of behaviour are calculated. (i) At low temperatures flow is predominantly governed by dislocation glide. This gives rise to work hardening over the whole strain range and limited strain rate sensitivity. (ii) As the temperature increases a transition to predominantly creep controlled deformation occurs. In this regime strain rate sensitivity markedly increases and the stress strain curve changes form, now showing initially, only slight work hardening, then a subsequent region where flow stress

remains relatively constant followed by work softening. (iii) There is a further intermediate regime as the low temperature behaviour transitions to creep controlled. In this case there is the possibility of considerable work hardening before strength values rise above the point where creep controlled deformation is the weakest mechanism. At this point work softening occurs. This is demonstrated in Fig.4.

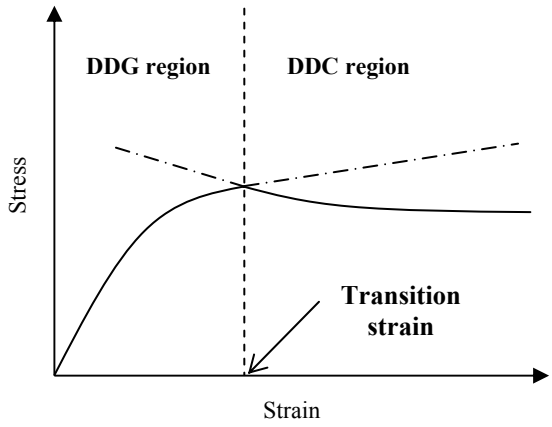

Figure 4. Change of deformation mechanism from DDG to DDC in a high temperature stress-strain curve at the critical transition strain (ε_t)

Comparison of calculated and experimental flow stress curves for alloy 718 at 1050°C are shown in Fig.5. At strain rates of 0.01 and 0.1 s^{-1}, flow stress is completely controlled by creep. At 1 s^{-1} the alloy first yields plastically via dislocation glide at 234 MPa. It then work hardens rapidly until at 263 MPa it can flow more easily by dislocation climb. Although the calculated work hardening is more rapid than shown by experiment, the agreement with creep controlled behaviour is very good.

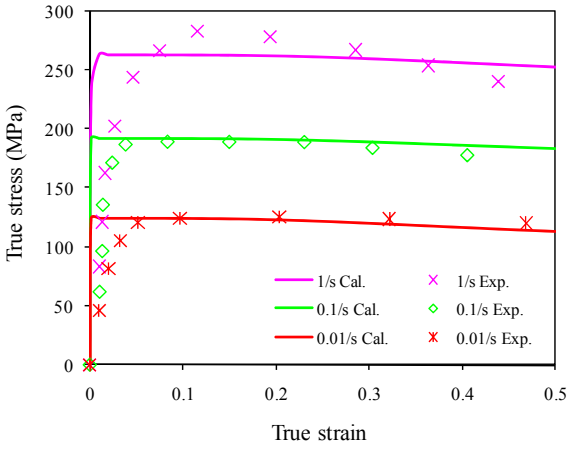

Figure 5. Comparison of calculated and experimental stress-strain curves for alloy 718 at 1050°C

Flow stress curves for 718 have been reported by a number of workers [14,15,16,17] and experimental work has also been reported for the well-known alloys 706 [18] and 800H [19,20]. Figs.6-8 show comparison of calculated and experimentally observed flow stresses, taken at various strains between 10% and 60%, over a wide range of temperatures and strain rates.

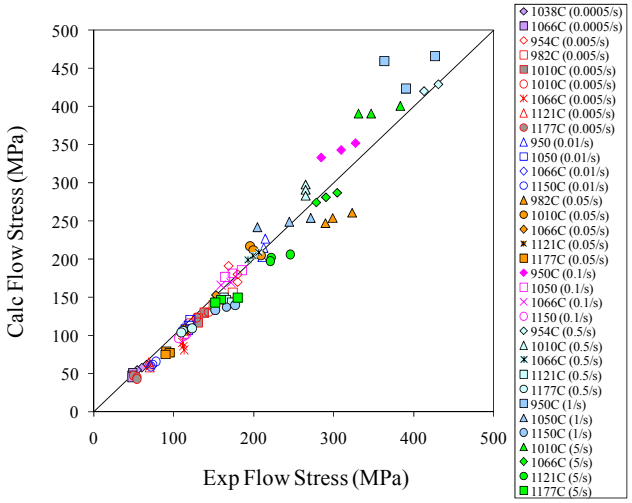

Figure 6. Comparison between calculated and experimental [14,15,16,17] flow stress for alloy 718

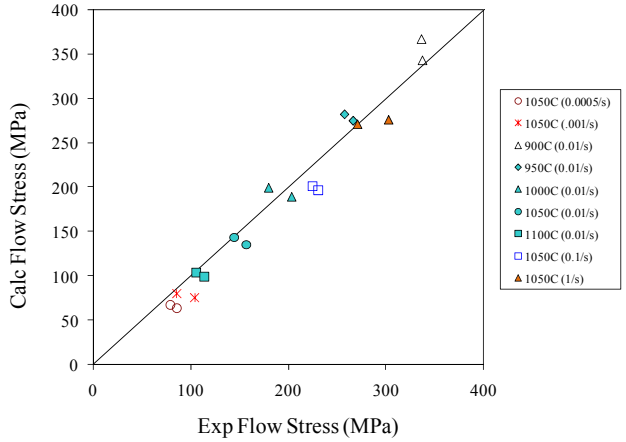

Figure 7. Comparison between calculated and experimental [18] flow stress for alloy 706

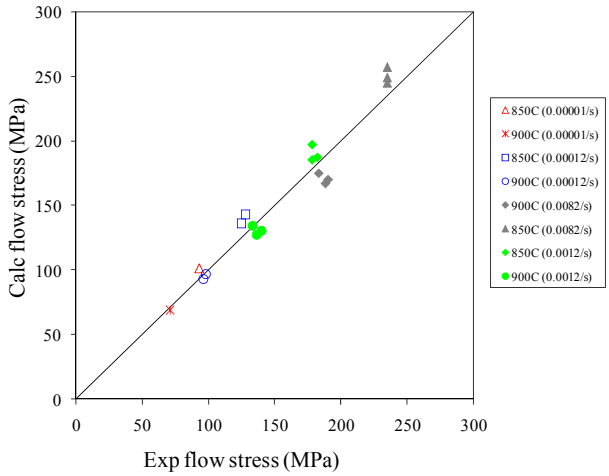

Figure 8. Comparison between calculated and experimental [19,20] flow stress for alloy 800H

The results of the calculations are extremely encouraging. Although it is often argued that flow softening is mainly controlled by recovery and recrystallisation process, it is clear that extremely good agreement with experiment is found using a creep model for a wide variety of alloy types, including various types of steel and Ti-alloys, in addition to Ni-based superalloys. In particular for steels, the experimentally observed onset of flow softening is matched very well.

This raises the question as to whether the onset of recovery and recrystallisation processes is the fundamental cause of flow softening. The modelling of flow softening, when using recovery and recrystallisation models, is invariably a process of fitting to specific experiment and cannot be easily generalized such that a predictive methodology results. This is not the case for the present work, which is predictive in nature and clearly linked to an existing and successful model for creep.

It must also be seriously questioned as to whether recovery and recrystallisation can occur at the higher strain rates, for example greater than 1 s^{-1}. The current model has been shown to successfully handle strain rates much higher than this, even up to 100 s^{-1} in Ti-6Al-4V [12,13], placing it close to ballistic strain rates. The present model is also far more practical for use in simulation of thermo-mechanical processing as it does not require modelling of recovery and recrystallisation to be included as an a-priori requirement for strength to be predicted.

Low Cycle Fatigue of Hastelloy X and Haynes 230

It has been said that 80~90% of all the structural failures occur through a fatigue mechanism [21]. The big challenge for modellers has therefore been to deliver reliable fatigue-analysis tools which help prevent "over-design" of components and yet ensure reliable life. Software packages are available that can be used for fatigue simulation of components or systems, but they all require the a-priori inclusion of fatigue properties, such as stress-life (S-N) or strain-life (ε-N) curves. However, it is often difficult to gain access to measured cyclic properties, as the number of alloys where such information is available is limited and it is problematic to experimentally measure all the required cyclic properties for generalised use.

One way to consider solving this problem is to relate cyclic properties to monotonic tensile properties. If estimation methods with reasonable accuracy can be established, fast solutions to fatigue problems can be provided without the time and cost involved in fatigue testing. Therefore, much effort has been put into finding such methods [22,23,24]. However, such attempts have invariably been empirical, providing some approximations that can be useful for specific problems, but not predictive in nature.

The ultimate way to solve this problem would be through computer modelling, where fatigue properties can be calculated as a function of alloy chemistry, processing details and working environment. This would be a significant step towards "true" virtual engineering design, where the design of components/systems and alloy composition/processing route are combined.

The first step of the present modelling approach has therefore been to calculate monotonic properties, which include yield/tensile strength, hardness, Young's modulus and stress-strain curves of commercial alloys as a function of alloy chemistry, processing details, strain rate and temperature. These properties can then be used in existing models used to describe cyclic stress-strain behaviour and strain-life relationships.

We have then used the classical Coffin-Manson equation to describe the strain-life behaviour:

$$\frac{\Delta\varepsilon}{2} = \frac{\sigma_f'}{E}(2N)^b + \varepsilon_f'(2N)^c \qquad (4)$$

Where, in an axial fatigue test, Δε is the total strain amplitude, N is the number of cycles to failure, E is the Young's modulus, σ_f' and b are, respectively, the axial fatigue strength coefficient and exponent and ε_f' and c are, respectively, axial fatigue ductility coefficient and exponent.

Almost all previous work on using the Coffin-Manson equations for estimating cyclic material properties from monotonic tensile test data has assumed that E is already known and that the four material parameters σ_f', ε_f', b and c must be estimated from other experimentally measured data. Meggiolaro and Castro [24] recently reviewed the available approaches and many evaluations have been carried out applying these approaches to various types of engineering alloys (e.g. 23,25,26,27,28). By using JMatPro to calculate σ_f', ε_f' and E it is possible to reduce the number of unknowns, leaving only b and c to be estimated. Two applications to Ni-based superalloys are presented below.

For the present study two solid solution alloys have been taken, Hastelloy X and Haynes 230. For both alloys, fully reversed pull-push (R = -1) fatigue tests were performed in air [29,30] with a frequency of 1 Hz, at temperatures between 816 and 982°C. The imposed axial total strain range was 0.4 to 2.0%, with corresponding equivalent strain rates of 0.008 to 0.04 s^{-1}.

For the sake of simplicity, an average value for the strain rate for was taken to be 0.02 s^{-1} and we have assumed $\sigma_f' = \sigma_{uts}$ and $\varepsilon_f' = \varepsilon_f$. From these values we have assessed temperature independent values for b and c of -0.07 and -0.9 for Haynes 230 and -0.07 and -0.75 for Hastelloy X. Δε-N curves have then been calculated and results compared with experiment (Fig.10) giving very satisfactory agreement.

The advantages of such calculations are very clear. Firstly it is possible to extend the Δε-N curves to a higher number of cycles (>10000) and, because b and c are temperature dependent, it is possible to calculate, at will, Δε-N curves for temperatures where no experiment has been undertaken.

It is also interesting to note that b has the same value for both alloys and the value for c is rather similar for both cases. It is interesting, therefore, to discover whether this would be a general case for all Ni-based superalloys. If so, there is significant potential to extend the current work to make very reasonable a-priori predictions for fatigue properties without recourse to experiment.

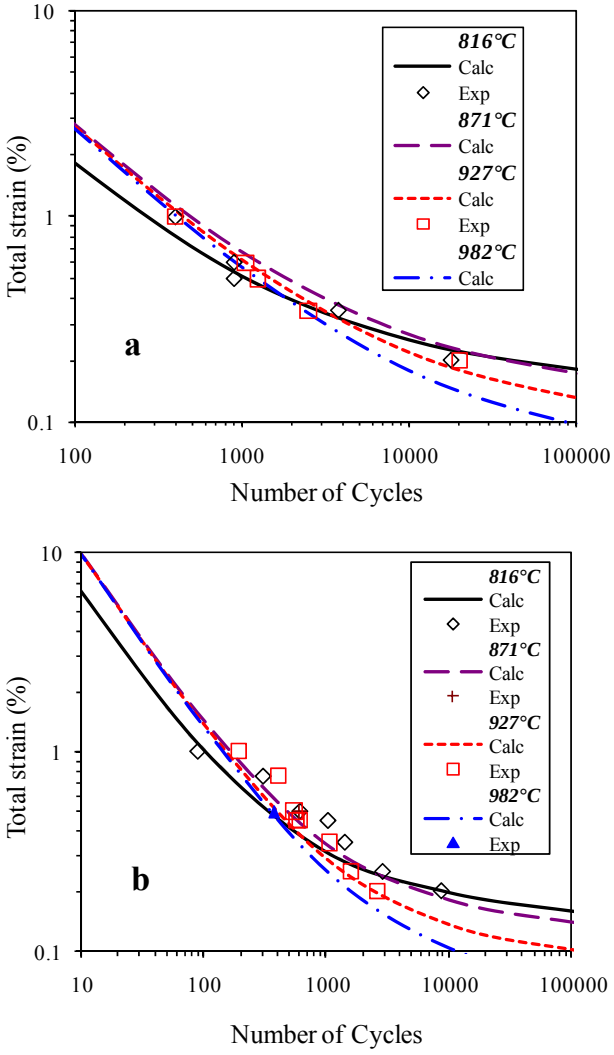

Figure 10. Comparison between experimental [29,30] and calculated Δε-N curves for (a) Hastelloy X and (b) Haynes 230 at different temperatures

Modelling the Evolution of γ′ Microstructure

Previous publications [3,31] have described the modelling of kinetic transformations for phases in Ni-based superalloys including various topologically close packed (TCP) phases as well as γ' and γ". This has resulted in the general ability to calculate TTT and CCT diagrams for Ni-based superalloys of all types. A coarsening model has also been developed that allows calculation of coarsening rates for γ' and γ" to a high level of accuracy [32]. It is of clear interest to combine the kinetic models with coarsening calculations to estimate the evolution of γ' microstructure and subsequently link them with existing models for strength [3,4] as a function of particle size and morphology.

Kinetic model

The development of a modified Johnson-Mehl-Avrami model that can be generally applied to calculate phase transformations for a variety of material types has been previously presented [31,33]. The model allows the morphology of the precipitate to be considered as well as specifics associated with potential nucleant sites. For γ' precipitation a spherical particle is assumed and, for the case of steady state nucleation, the governing equations can be written as

$$X = \frac{V}{V_{eq}(T)} = 1 - \exp\left(-fN_r G_r^3 t^4\right) \quad (5)$$

Where X is the volume fraction of the product phase, V is the volume transformed, $V_{eq}(T)$ is the equilibrium volume amount of the phase at temperature T, f is a shape factor, with a value close to unity, N_r is the nucleation rate, G_r is the growth rate and t is time. For most cases, and especially so for γ', the volume difference between parent and product phases is similar enough such that volumes can be interchanged with mol.% values and V_{eq} in the present case is directly taken from the equilibrium mol.% calculation. For the case where site saturation occurs

$$X = 1 - \exp\left(-fN_o G_r^3 t^3\right) \quad (6)$$

Where N_o is the total number of active nucleant sites. The method for calculating N_r and G_r has been described in detail by Li et al. [33] and all required information can be obtained from thermodynamic calculation and diffusional databases within JMatPro. For γ', N_o is taken as between 10^{22}-10^{23} m^{-3}, similar to that which can be observed in Ni-Al binary alloys [34]. In this case, the start of transformation is associated with particles of approximately 5nm in size, which would produce sufficient strengthening to allow a comparison to be made with TTT diagrams derived from hardness measurements [3,31,35].

As is known from practice, the formation of γ' is very rapid, with little undercooling below the γ' solvus required before transformation occurs. This rapid transformation also means that site saturation is rapidly achieved and, for all of the current work, it is Eq. 6 that appears to be the ruling equation.

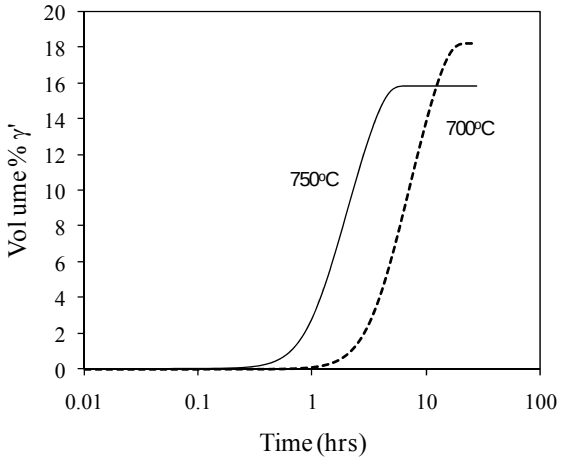

Figure 11. Calculated vol.% γ' formed at 700 and 750°C in Nimonic 80A

Eqs. 5&6 are isothermal in nature and can be used directly to calculate the evolution of volume fraction (V_f) vs. time at a constant temperature and Fig.11 shows such calculations for Nimonic 80A at 700 and 750°C. It is interesting to note that transformation for both cases are virtually complete in the time

provided by the heat treatment schedules, 4 and 16hrs respectively for 750 and 700°C. In all the cases described here, transformation is either complete, or almost fully complete, within the time frame of the isothermal treatment schedule.

For the particular case of heat treatment at 700 and 750°C, little or no coarsening takes place, as coarsening rates are too low. The γ' particle volume can effectively be estimated by simply dividing V by N_o. For alloys where transformation occurs below 800°C during a one-step hardening treatment we have calculated particle diameters which can then be compared with experiment (Table 1).

Table 1. Comparison between experimentally reported [6] and calculated γ' sizes in some Nimonic alloys

Alloy	γ' diameter (nm)	
	Exp	*Calc*
Nimonic 80A	20	20
Nimonic 90	20	20
Nimonic 263	22	16
Nimonic PE11	18	18
Nimonic PE16	18	14

These are rather simple examples. With temperatures involved in practical heat treatment schedules, coarsening of γ' must be taken into account both during isothermal transformations and cooling.

Inclusion of coarsening

The simplest method to include coarsening, for both isothermal and cooling transformations, is to first calculate X using Eqs. 5&6 and apply simple additivity rules [36]. Transformation is calculated for discrete time intervals and a sum of fraction transformed is obtained. For an isothermal case the transformation occurs at a constant temperature, with constant values for $V_{eq}(T)$, N_r and G_r. For continuous cooling, small isothermal steps are taken and $V_{eq}(T)$, N_r and G_r calculated for each temperature.

The procedure adopted is to (i) calculate the transformation in the discrete time interval at a constant temperature and (ii) calculate coarsening. In cooling the time interval is chosen to correspond to a chosen cooling rate. In the first stages of the procedure, the size of γ' is simply calculated using V and either the number of nuclei formed during steady state nucleation or, when site saturation occurs, by using N_o. However, at some point the combination of coarsening rates and time will allow γ' to coarsen. Invariably, we have found that for all transformation where coarsening occurs, conditions for site saturation have been achieved and Eq. 6 becomes the ruling equation. The effect of coarsening is to reduce the number of γ' particles, effectively reducing the value of N_o in Eq. 6 . At the next step a new value for N_o is calculated from V and the coarsened particle diameter.

We have also found that, when coarsening rates are high, a simple application of coarsening during the early stages of transformation leads to highly inaccurate predictions for size - in all cases calculated particle sizes are far higher than observed. This may be because, in the early stages of transformation, diffusion fields surrounding the γ' particles are small with no overlap between surrounding γ' particles. For coarsening to occur, mass transport between γ' that is shrinking and γ' that is coarsening is required. To this end we do not consider coarsening can be effective until overlap of the diffusion fields of γ' particles occurs.

The exact description of composition gradients with overlapping diffusional fields is complex and beyond simple analytical equations. However, if the effect of complex gradients is second order, in comparison to the requirement of overlap, a simple procedure may suffice to account for a "delayed" onset of coarsening. To this end calculations have been made such that when $\sqrt{Dt}$ is of the order of an interparticle spacing, coarsening occurs. Including such a term immediately provides more realistic answers.

The effect of reducing N_o is to reduce the transformation rate, which does raise the possibility that increased supersaturation of the matrix may allow for new nucleation events to occur. In which case, "secondary" γ' may form between the γ' particles formed during the "primary" transformation. There is evidence to suggest that this takes place on cooling, see for example Mao et al. [37] and Mitchell et al. [38]. But, it is noted that such "secondary" formation of γ' was only observed at cooling rates $<0.5\ s^{-1}$. In the present work, this secondary burst is not considered, though work is on-going to include secondary nucleation and growth. However, the inclusion of such a phenomenon may not be critical for the primary aim of the work, which is to link microstructure prediction with mechanical property calculations and hence predict strength as a function of heat treatment schedule.

Results and discussion

While Fig.11 showed results for vol.% γ' vs. time for the isothermal transformation, Fig.12 shows vol.% γ' vs. temperature for a U720LI alloy on cooling from a super-solvus heat treatment at 1168°C. Three cooling rates are shown, 0.5, 1 and 5 °C s^{-1}, with associated calculated γ' particle diameters.

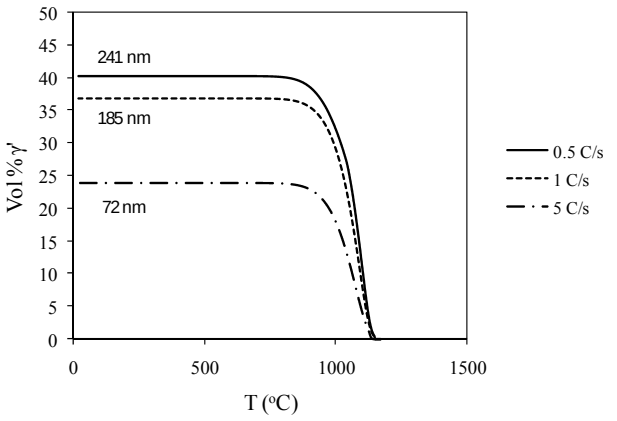

Figure 12. Calculated vol.% γ' formed in U720LI during cooling at various rates with calculated γ' particle diameters included.

The effect of including coarsening during cooling, is that there is an initial rapid increase in the γ' particle diameter at very low volume transformed. This appears as much due to the rapid rate of coarsening of very fine γ' particles as to the high coarsening rates existing at temperature. The effect of coarsening on γ' size reduces quite rapidly, and γ' particle diameter then increases almost exclusively by growth of γ' particles due to the increasing volume of γ' that is formed (Fig.13).

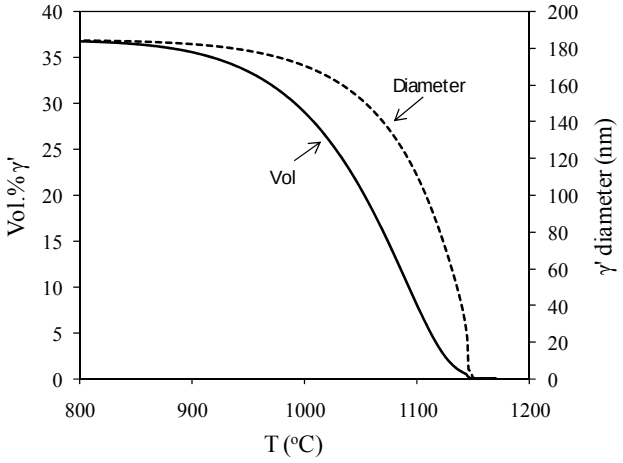

Figure 13. Calculated vol.% and diameter of γ' formed in U720LI during cooling at 1 °C s^{-1}.

Recently, systematic studies have been undertaken to experimentally determine the γ' size and distribution as a function of cooling rate [37,38,39] and Fig.14 shows the comparison between these experiments and calculation. In the work of Mitchell et al. [38] two of their cooling rates are given as being between 10-15°C s^{-1} and between 1-2 °C s^{-1}. Calculations have been made for the case of the extremes, which should bracket experiment. In the case of Mao et al. [37], alloys cooled at 0.46 and 0.18 °C s^{-1} exhibit some bi-modal behaviour. Fig.14 shows comparison between both sizes.

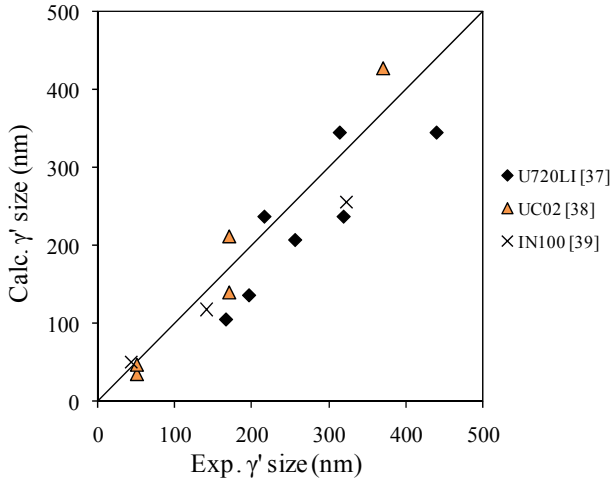

Figure 14. Comparison between calculated and experimentally observed γ' sizes formed at various cooling rates

It is now possible to use the model to calculate γ' distribution as a function of heat treatment schedule for at least the case of a two-stage heat treatment, i.e. a high temperature anneal, followed by cooling to room temperature and a subsequent isothermal treatment to generate maximum strength. For the case where γ' forms on cooling, a simple mass balance calculation that takes into account the amount of γ' that has formed, provides the composition of γ for the isothermal stage. Using the calculated amounts and distribution of γ', both 0.2% proof stress and UTS can then be calculated using strength models reported previously [3,4,31].

Mao et al. [37] determined strengths for U720LI, both after cooling from 1068°C at various rates and also after subsequent heat treatment at 700°C for 24hrs. Fig.15 shows a comparison between experimentally measured 0.2% proof stress and UTS and the current calculations.

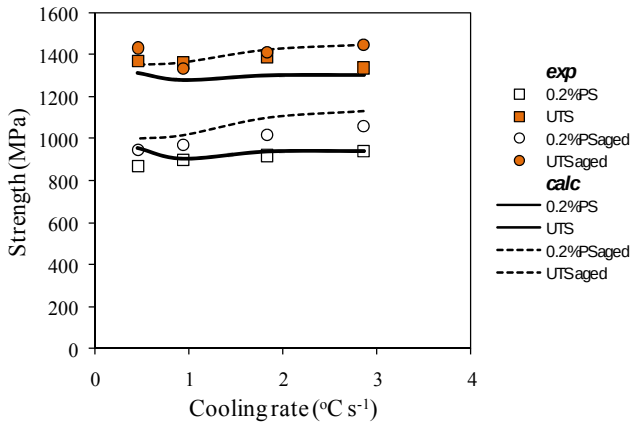

Figure 15. Comparison between calculated and experimentally observed strength [37] of U720LI (i) cooled at various rates and (ii) subsequently aged at 700°C for 24 hrs.

The calculations compare well with experiment. It is interesting to note that the calculated unaged 0.2% proof stress at the lowest cooling rate (0.46 °C s^{-1}) is slightly higher than at 0.94 C s^{-1}. This is because the increase in size, which will weaken the alloy, is offset by the increase in the amount of γ', which strengthens the alloy. The strength as a function of cooling rate will not be a simple function, as both the change in strength as a function of size ($d\sigma/d$size), as well as the change in strength as a function of volume ($d\sigma/d$vol) are, in themselves, not simple functions. In this light it is interesting to note that the experimentally observed UTS does follow the trend as calculated.

It is now instructive to compare calculated strengths as a function of heat treatment for a series of commercial wrought alloys which have been given two-stage heat treatments. Also included are three simple as-cast alloys, where the assumption has been made that they are fully γ before γ' precipitation. In future it should be possible to consider more complex cases, but for the purpose of the present validation, the alloys used suffice to demonstrate capability.

The cooling stage for all but one of the wrought alloys is air cooling and we have taken 1 °C s^{-1} to represent the rate. This is in keeping with known cooling rates for air cooled round steel bars of approximately 2 in. diameter [40]. For the cast alloys a rate of 0.333 °C s^{-1} has been used. For two alloys, Nimonic 115 and N18, although one and two-stage treatments are essentially used in the calculations, their heat treatment is more complex. However, they are included as the heat treatment procedure can be modelled using a simple additional coarsening stage and particle size information exists for both alloys. For all alloys, both 0.2% proof stress as well as UTS are calculated and compared with those reported experimentally [6,41.42] (Fig.16).

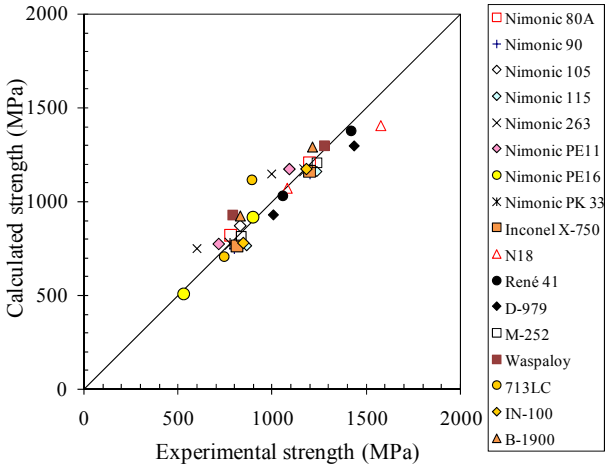

Figure 16. Comparison between calculated and experimentally reported strengths [6,41,42] , of various Ni-based superalloys

Nimonic 115 is first super-solvus annealed, followed by air cooling to RT. It is then given a sub-solvus treatment where γ' remaining from cooling is coarsened to ~500 nm. It is subsequently air-cooled and a fine γ' precipitation is formed, giving a bi-modal particle distribution. To model this process, the particle size from super-solvus cooling was first calculated, before a simple coarsening calculation was made for the sub-solvus treatment. γ' precipitation during cooling from the sub-solvus treatment is then calculated. Predicted particle sizes are 409 and 129 nm, while experimentally they are ~ 500 and 100 nm respectively.

For N18, a sub-solvus treatment is the first stage, where coarse γ' of size ~4000 nm is retained [42,43]. The alloy is then cooled at 1.67 °C s^{-1} to room temperature [42] and a two-stage hardening treatment applied, the first stage is at 700°C followed by a second heat treatment at 800°C. For the current calculation, γ' calculated to form at 700°C is reduced slightly in amount to equilibrium at 800°C and allowed to coarsen. Particle sizes of 160 (formed on cooling) and 41 nm (formed on isothermal heat treatment) are calculated in comparison to that observed on cooling of 130nm [42] and 210nm [43] and on heat treatment of 20nm [43]. Reported strengths used in the comparison are from Ducrocq et al. [42] and we have used 4000 nm as the size of the coarse γ'.

For Nimonic 105, an isothermal treatment at 850°C is applied after cooling from a supersolvus heat treatment. Almost all of the γ' precipitation takes place during the isothermal treatment and significant coarsening occurs, producing a calculated γ' diameter of 68 nm in comparison to that experimentally observed [6] of 70 nm.

Considering the potential complexity of the model which combines thermodynamic, kinetic, coarsening and strength modelling, the procedure is essentially simple, utilising already existing models, with only one further term, the time to onset of coarsening, needing to be evaluated. As such, the level of agreement between calculation and experiment is extremely good, providing confidence to extend the approach to more complex heat treatment and potentially integrating with process simulation packages to predict detailed final properties of components.

Summary

The present paper reports on models for (i) the calculation of flow stress diagrams as a function of strain rate and temperature and (ii) the calculation of γ' microstructure resultant from heat treatment and casting.

For the case of flow stress diagrams it has been shown that flow softening can be accounted for by using strength models that include creep as a controlling factor at high temperatures. This has very significant advantages, in that process models do not need to include additional models for recovery and recrystallisation to account for the phenomenon, and can utilise existing data input formats.

An application to fatigue has been made, whereby the number of experiments necessary to evaluate coefficients for the Coffin-Manson equation can be significantly reduced. The current results suggest an interesting possibility that all necessary input could be made a-priori, hence allowing a predictive capability for calculating Δε-N curves. Further work will be undertaken to evaluate whether this is possible.

Previous models for calculating the formation of γ' have been extended to include coarsening. This has allowed the prediction of γ' microstructure as a function of heat treatment. Transformation both isothermally and on cooling is considered and detailed comparison with experimental observation has been made. The resultant γ' microstructures have been linked with previously reported strength models to calculate RT strength. Extensive comparison with experiment has been made where agreement is highly satisfactory.

The current work extends previous capability of the software JMatPro such that, it is now possible, in combination with existing simulation software for solidification processing, forging and heat treatment, to consider the true "virtual" design of components on computer, without the need for extensive experimentation to measure material properties, microstructures and/or strengths resulting from imposed heat treatment schedules.

References

1. N. Saunders, *Superalloys 1996*, eds. R. Kissinger et al. (Warrendale, PA: TMS, 1996), 115.
2. N. Saunders, M. Fahrmann and C.J. Small, *Superalloys 2000*, eds. K. A. Green et al (Warrendale, PA: TMS, 2000), 803.
3. N. Saunders, Z. Guo, X. Li, A.P. Miodownik and J-Ph. Schillé, *Superalloys 2004*, eds. K. A. Green et al (Warrendale, PA: TMS, 2004), 849.
4. Z. Guo, N. Saunders, A.P. Miodownik and J-Ph. Schillé, *Materials Science Forum*, 546-549 (2007), 1319.
5. A.P. Miodownik, X. Li, N. Saunders and J.-Ph. Schillé, *Parsons 2003: Engineering Issues in Turbine Machinery, Power Plant and Renewables,* eds. A. Strang et al., (London: Inst.MMM, 2003), 779.
6. W. Betteridge and J. Heslop, *The NIMONIC Alloys and Other Ni-Base High Temperature Alloys: 2nd ed.*, (London: Edward Arnold Ltd, 1974)

7. *Special Metals Product Handbook of High-Peformance Alloys*, Publication No. SMC-035, (Huntington, WV: Special Metals Corporation, 2001).
8. X. Li, A. P. Miodownik and N. Saunders, *J. Phase Equilibria*, 22 (2001), 247.
9. J.C.M. Li, *Acta Metall.*, 11, (1963), 1269.
10. F. Garofalo, W.F. Domis and F. Von Gemmingen, *Trans.Met.Soc.AIME*, 230 (1964), 1460.
11. R. Lagneborg and B. Bergman, *Met. Science*, 10 (1976), 20.
12. N. Saunders, Z. Guo, A.P. Miodownik and J-Ph. Schillé, *presented at the 5th Int.Conf. on Physical and Numerical Simulation of Materials Processing, ICPNS'2007,* Zhengzhou, China, Oct 23-27 2007
13. N. Saunders, Z. Guo, A.P. Miodownik and J-Ph. Schillé, *submitted for publication in Mat.Sci.Eng.A*
14. M.J. Weis, M.C. Mataya, S.W. Thompson and D.K. Matlock, *Superalloy 718*, ed. E.A. Loria, (Warrendale, PA: TMS, 1989), 135.
15. C.I. Garcia, G.D. Wang, D.E. Camus, E.A. Loria and A.J. DeArdo, *Superalloys 718,625, 706 and Various Derivatives*, ed. E.A. Loria, (Warrendale, PA: TMS, 1994), 293.
16. D. Zhao, S. Guillard and A.T. Male, *Superalloys 718,625, 706 and Various Derivatives*, ed. E.A. Loria, (Warrendale, PA: TMS, 1997), 193.
17. N.K.Park, J.T. Yum, Y.S. Na, I.S. Kim, D.H. Kim and S.J. Choe, *Superalloys 718,625, 706 and Various Derivatives*, ed. E.A. Loria, (Warrendale, PA: TMS, 1997), 173.
18. Z. Long, D. Fu, P. Ma, Z. Zhong, *Superalloys 718,625, 706 and Various Derivatives*, ed. E.A. Loria, (Warrendale, PA: TMS, 1997), 205.
19. H. Cords and R. Zimmerman, *Computer and Structure*, 44 (1992), 1.
20. M.E. Abd El-Azim, *J.Nucl.Mater.*, 231 (1996), 146.
21. J.J. Duga, W.H. Fisher, R.W. Buxbaum, A.R. Rosenfield, A.R. Buhr, E.J. Honton, and S.C. McMillan, *Int.J.Fracture*, 23 (1983), R81.
22. K.S. Kim, X. Chen, C. Han and H.W. Lee, *Int.J.Fatigue*,24 (2002), 783.
23. K.S. Lee and J.H. Song, *Int.J.Fatigue*, 28 (2006), 386.
24. M.A. Meggiolaro and J.T.P. Castro, *Int.J.Fatigue*, 26 (2004), 463.
25. K.S. Kim, X. Chen, C. Han and H.W. Lee, *Int.J.Fatigue*, 24 (2002), 783.
26. M.L. Roessler and A. Fatemi, *Int.J.Fatigue*, 22 (2000), 495.
27. J.H. Ong, *Int.J.Fatigue*, 15 (1993), 13.
28. J.H. Ong, *Int.J.Fatigue*, 15 (1993), 213.
29. Y.L. Lu, L.J. Chen, G.Y. Wang, M.L. Benson, P.K. Liaw, *Superalloys 2004*, eds. K. A. Green et al (Warrendale, PA: TMS, 2004), 241.
30. Y. L. Lu, L. J. Chen, G.Y. Wang, M.L. Benson, P.K. Liaw, S.A. Thompson, J.W. Blust, P.F. Browning, A.K. Bhattacharya, J.M. Aurrecoechea, D.L. Klarstrom, *Mater.Sci.Eng.A,* 409 (2005), 282.
31. N. Saunders, X. Li, A.P. Miodownik and J-Ph. Schillé, *Materials Design Approaches and Experiences*, eds. J.-C. Zhao et al., (Warrendale, PA:TMS, 2001), 185
32. X. Li, N. Saunders and A.P. Miodownik, *Metall.Mater.Trans.A*, 33A (2002), 3367.
33. X. Li, A.P. Miodownik and N. Saunders, *Mater.Sci Tech.*, 18, (2002), 861.
34. H.I. Aaronson and F.K. LeGoues, *Met.Trans.A*, 23A (1992), 1915.
35. N. Saunders, Z. Guo, A.P. Miodownik, J-Ph. Schillé, *Superalloys 718, 625, 706 and Derivatives 2005,* Ed. E.A. Loria ((Warrendale, PA: TMS, 2005), 571.
36. J. S. Kirkaldy, Scand. J. Metall., 20 (1991), 50.
37. J. Mao, K.-M. Chang, W. Yang, K. Ray, S.P. Vaze and D.U. Furrer, *Met.Mater.Trans.A*, 32A (2001), 2441.
38. R.J. Mitchell, M.C. Hardy, M. Preuss and S. Tin, *Superalloys 2004*, eds. K. A. Green et al (Warrendale, PA: TMS, 2004), 361.
39. A.M. Wusatowska-Sarnek, M.J. Blackburn and M. Aindow, *Mater.Sci.Forum*, 426-432 (2003), 767.
40. M. Atkins, *Atlas of Continuous Cooling Transformation Diagrams for Engineering Steels,* (Sheffield: British Steel Corporation, 1977).
41. *Superalloys 2,* eds. C.T. Sims, N.S. Stoloff and W.C. Hagel (New York: John Wiley & Sons, 1987)
42. C. Ducrocq, A. Lasalmonie and Y. Honnorat, *Superalloys 1988*, eds. S. Reichman et al (Warrendale, PA: TMS, 1088), 63.
43. S.T. Wlodek, M. Kelly and D. Alden, *Superalloys 1992*, eds. S.D. Antalovich et al (Warrendale, PA: TMS, 1992), 467